DUCTED CO-ROTATING ROTORS AS AN ALTERNATIVE FOR UAV PROPULSION: AN EXPERIMENTAL AEROACOUSTIC STUDY

Pawel Kekus-Kumor
Łukasiewicz Research Network — Institute of Aviation
Warsaw, Poland

Adam Sieradzki
Łukasiewicz Research Network — Institute of Aviation
Warsaw, Poland

ABSTRACT

The coaxial, co-rotating configuration of rotors, also referred to as stacked rotors, is a promising alternative to counter-rotating rotors, simpler and lighter mechanically, while still providing improved disk loading relative to an isolated rotor. Ducting, on the other hand, is commonly used on rotorcraft for improved efficiency and safety, as well as some reduction of noise emissions. In this work, the two solutions are combined. Aeroacoustic performance of ducted stacked rotors is evaluated experimentally in an anechoic chamber, and compared to similar cases of an isolated rotor, a single ducted rotor, and unducted stacked rotors. Although changes to blade geometry necessitated by the presence of a duct prevent testing of truly analogous cases, an attempt is made at a fair comparison between the different configurations. The results show similar efficiency of the ducted stacked configuration relative to a single ducted rotor, but with an apparent detriment to the acoustic performance. Compared to unducted stacked rotors, the ducted configuration provides improved efficiency and similar noise levels. Furthermore, a range of blade pitch angles, with varying increments between the upstream and downstream rotors, is tested for the ducted stacked rotors. The impact of dissimilar pitch between the rotors on the aeroacoustic performance of the system is small but distinct, with certain pitch configurations generating less noise than others. This suggests that there is significant potential in optimising rotor blades specifically for coaxial operation.

NOTATION

*

Symbols

C_Q Torque coefficient, -

C_T Thrust coefficient, -

f Frequency, Hz

L_{pA} A-weighted sound pressure level, $dB(A)$

Q Torque, Nm

R Rotor radius, m

T Thrust, N

β_r Relative blade pitch angle, $^\circ$

θ Angle relative to rotor plane, $^\circ$

ρ Air density, kg/m^3

ω Rotational speed, RPM

Ω Rotational speed, rad/s

*

Acronyms

BPF Blade passing frequency

DL Disk loading

ERF European Rotorcraft Forum

FM Figure of merit

Ł-ILOT Łukasiewicz Research Network — Institute of Aviation

PL Power loading

RPM Revolutions per minute

SPL Sound pressure level

UAV Unmanned air vehicle

INTRODUCTION

Unmanned aerial vehicles (UAVs) have become ubiquitous in both civilian and military applications, ranging from leisure activities, through aerial photography and photogrammetry, to logistics, surveillance and defence. Multirotor vehicles, which are particularly widespread in civilian operations, typically rely on electric power for lift and manoeuvrability, therefore optimising their propulsive efficiency is essential for increasing their range. Moreover, as their prevalence in urban and sensitive environments grows, so too does the importance of minimising their acoustic footprint. Noise emissions from UAVs not only affect public acceptance and regulatory compliance (Ref. 1, 2), but also influence mission effectiveness in certain applications. Consequently, the aeroacoustic performance of UAV propulsion systems has emerged as a key area of research and development (Ref. 3, 4).

The dominant source of noise in electric UAVs is the propulsion system, with a mechanical contribution from motors, and an aeroacoustic one from rotors or propellers. Rotor noise arises from a combination of tonal components, primarily related to the blade-passing frequency (BPF) and its harmonics, and broadband components, mainly associated with turbulence (Ref. 5, 6). Key mechanisms of noise generation include leading edge interaction with incoming turbulence, blade tip vortices, and the interaction of the boundary layer on blade surfaces with the trailing edge (Ref. 5, 6). While computational tools for modelling these phenomena have advanced over time, experimental measurements remain essential for validating these models and capturing real-world performance, particularly in configurations involving complex interactions (Ref. 5).

A variety of rotor configurations are used in UAV propulsion, each with distinctive aerodynamic and acoustic characteristics. The simplest is a single rotor per propulsion unit, which is straightforward mechanically, lightweight and cost-effective. However, single rotors achieve relatively low disk loading, i.e. thrust per surface area, which may lead to relatively large rotor diameters and vehicle dimensions, with a negative impact on their portability and manoeuvrability.

To address this, coaxial rotor systems are often employed, where two rotors are mounted on a single axis, either on top of each other, or on opposite sides of the motor(s). There are three primary configurations of coaxial rotors:

- Co-rotating, or stacked, where two rotors are mounted on a single shaft, and therefore rotate at equal rotational velocities, with a fixed azimuthal separation (index angle). This separation is often fixed at 90°, but may vary as well (Ref. 7–10). The advantages of this configuration are its mechanical simplicity and good thrust-to-noise performance (Ref. 7, 8).

- Contra-rotating, where two rotors are propelled by the same motor, but one of them in the opposite direction thanks to a mechanical gear system (Ref. 11). While still requiring only one motor, the gearing results in additional weight and complexity compared to co-rotating (stacked) rotors. The main advantage of this configuration is the increased aerodynamic efficiency, in part due to swirl reduction, but this comes at the cost of increased noise emissions due to the interaction of the downstream rotor with the wakes of the upstream blades (Ref. 11, 12).

- Counter-rotating, where two rotors are powered by individual motors, enabling more precise control of the aircraft's attitude. The heaviest of the three configurations due to the additional motor and control electronics, counter-rotating rotors also have the most complex acoustic signature, due to the variable phase between rotors in each propulsion unit (Ref. 12).

All of these configurations provide higher disk loading than a single rotor, enabling more compact UAV designs, which is particularly valuable in constrained environments, such as during indoor or urban operations.

Another approach to improve the characteristics of UAV propulsion systems is the use of ducts around rotors. The presence of a shroud in close proximity to rotor tips suppresses the formation of tip vortices, and the induced airflow over the duct generates additional thrust, and with greater efficiency than rotors (Ref. 13, 14). Ducts can also serve as acoustic shields, attenuating noise propagation in certain directions (Ref. 14–17). Furthermore, operational safety of the UAVs is improved, as ducts reduce the likelihood of accidental contact of rotor blades with the surroundings. However, the addition of ducting introduces a number of challenges, including structural complexity, added weight, and the risk of flow separation off the duct's lip (Ref. 14, 18), which leads to a performance degradation. Furthermore, the interaction of blade tips with the boundary layer on the duct's internal surface introduces a new source of noise (Ref. 19).

Stacked ducted rotors represent a hybrid configuration that combines the benefits of coaxial and ducted systems. In theory, this arrangement could offer high thrust density and improved noise shielding, making it attractive for compact UAVs operating in noise-sensitive environments. Despite these potential benefits, the aeroacoustic behaviour of such systems remains poorly characterised.

This study aims to address this gap by providing a systematic experimental comparison of four UAV rotor configurations: an isolated rotor, stacked (coaxial, co-rotating) rotors, a single ducted rotor, and stacked ducted rotors. Furthermore, the potential of utilising dissimilar pitch for stacked rotors is examined. Although comparing ducted and unducted systems is made difficult by the necessarily distinct blade geometries in the two cases, this study is an attempt to provide a sufficiently fair comparison to enable conclusions to be drawn. The results presented herein are intended to inform researchers and engineers about the relative merits of each configuration, and to lay groundwork for more extensive research in the future.

In the sections that follow, we describe the experimental setup and measurement methodology, followed by a presentation of the aerodynamic and acoustic results for all four rotor configurations. Next, we present data for stacked ducted rotors with dissimilar pitch, evaluating the potential of this solution. Finally, we conclude with a summary of key observations and recommendations for further research.

METHODOLOGY

The aim of this study was to investigate aeroacoustic characteristics of several rotor configurations, therefore a suitable acoustic environment was required, as well as appropriate measurement rigs. Due to the lack of an anechoic wind tunnel at the Łukasiewicz Research Network — Institute of Aviation (Ł-ILOT), the testing campaign was constrained to the hover condition, which could be tested in an enclosed anechoic chamber. Although this narrows the scope of this study, the data and trends presented in this work can be related to the vast volume of literature on UAV rotor systems in hover (e.g. Ref. 8, 9, 11, 16, 17, 20).

All the data presented in this paper was obtained in the anechoic chamber at Ł-ILOT. The chamber is a freestanding room built using a drywall system, filled with mineral wool and lined with high-density plasterboard. The chamber rests on an array of vibration isolators and is equipped with an acoustic door and acoustically sealed cable channels. The interior of the chamber, including the floor and the door, is lined with 0.5 m-high foam wedges, resulting in tip-to-tip dimensions of $3.40 \times 3.15 \times 4.00$ m. The average A-weighted background noise sound pressure level (SPL) inside the chamber is 18 dB, whereas the anechoic condition is satisfied down to 125 Hz, albeit with mild deviations at 315 Hz and below. More detail on the construction and acoustic validation of the chamber can be found in Ref. 21, 22.

The measurement rig used for testing the ducted and unducted rotors comprised two semi-independent subsystems. The rotor rig was based on a vertically-mounted steel tube with a 50 mm diameter, which located the rotors 1.3 m above wedge tips, and was equipped with an AXI 2814/28 V2 electric motor, a RiKO PRC-320 rotational speed sensor, an Octogon FSA-50 thrust sensor, and a FUTEK QTA143 torque sensor. The duct rig was based on an aluminium frame surrounding the rotor rig, with the duct positioned around the rotors by two arms. The arms, one on either side of the duct, were equipped with KD45 force sensors, in order to measure the thrust generated by the duct. The two rigs were joined together with an aluminium bracket roughly halfway up the rotor rig in order to help maintain concentric positioning of the rotors and the duct; this was the only point of contact between the two rigs above the ground. Both rigs are shown assembled in the anechoic chamber in Fig. 1 and 2, with the duct and a pair of rotors installed.

Acoustic measurements were carried out using an arc of PCB 378B02 free-field microphones, located at a radius of 1.2 m from the centre of the rotor hub. One microphone was mounted in the plane of the rotor ($\theta = 0°$), two were mounted upstream ($\theta = 20°$ and 40°), and three downstream ($\theta = -20°$, $-40°$ and $-60°$). The microphone arc can be seen

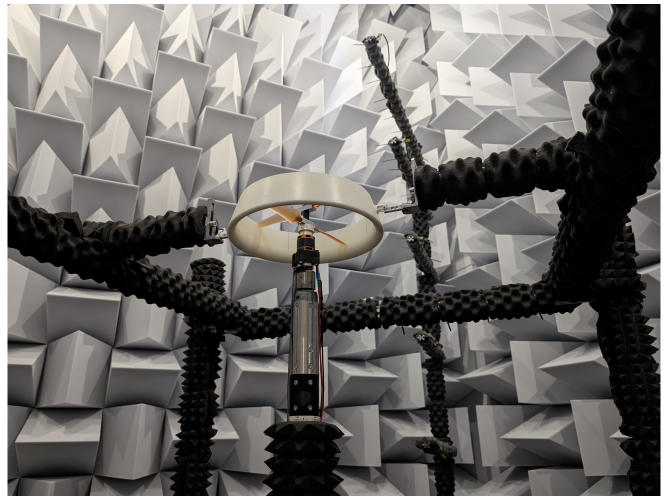

Figure 1: The fully assembled rotor testing rig in the anechoic chamber, with the duct and a pair of rotors installed.

Figure 2: A close-up of the rotor testing rig.

in Fig. 1. The data acquisition system consisted of two NI cDAQ-9189 chassis, with NI-9250 cards for the microphones and NI-9203 and NI-9205 cards for load, rotational speed and atmospheric sensors. Microphone signals were acquired at a frequency of 51.2 kHz, whereas the remaining data channels were acquired at 1 kHz. The signals were sampled for 5 s, with sampling commencing as soon as the rotational speed of the rotors stabilised at the target value, in order to avoid recirculation effects (Ref. 22). Microphone signals were split into 0.5 s-long, Hanning-windowed Welsh blocks for the calculation of power spectral density of the pressure signals, with a narrowband frequency of 20 Hz and an SPL reference pressure of 20 μPa used for all measurements. All SPL values are calculated from the spectra between 100 Hz and 20 kHz, which correspond to the operating range of the chamber, and are A-weighted.

The unducted configurations were tested using off-the-shelf APC rotors. The baseline was the 2-bladed 12x5.5MR rotor, which was used in conjunction with another 12x5.5MR rotor, as well as the 12x4.5MR variant, in the unducted stacked configuration. Because of the lack of suitable off-the-shelf components, the ducted stacked rotor configuration was tested using a custom duct and 2-bladed rotor geometries, designed for the study of single stacked rotor aeroacoustics. The duct had a length of 70 mm, an outer diameter of 300 mm, and a 42.8 mm-long internal section with a constant diameter of 260 mm, able to accommodate two coaxial rotors. The rotors were installed at a tip-to-tip axial separation of 30 mm (using a 20 mm separator), with the downstream rotor's trailing edge tip 7 mm upstream of the duct's exit. Although the duct and rotors were designed for a 1 mm tip clearance, the actual clearance when assembled on the rig was approximately 0.7 mm. Both the duct and the rotor blades were 3D-printed with resin, using digital light processing for the blades and stereolithography for the duct. Pairs of blades were mounted on machined aluminium hubs, which were mounted on a common shaft with a spacer in between. Detail of the duct and rotor assembly can be seen in Fig. 1 and 2. Stacked rotors were mounted at index angles of 90°, i.e. perpendicular to each other, both with and without a duct. Additional information about the design of the duct and the experimental setup was presented by Sieradzki, et al. (Ref. 23).

In order to evaluate the impact of dissimilar pitch on the performance of the ducted rotor system, additional blades were printed in several variants. In addition to the baseline geometry, designed for single-rotor operation (whose pitch angle is the reference point, i.e. a relative pitch of $\beta_r = 0°$), blade variants with relative pitch of $\beta_r = \pm1°$, $\pm2°$ and $\pm3°$ were printed. Two separate testing campaigns were carried out. In the first, all possible combinations of pitch angles on the upstream and downstream rotors were tested, as outlined in Table 1. Only increasing pitch in the streamwise direction was tested (i.e. downstream rotor pitch equal or higher to upstream rotor pitch, $\beta_{rD} \geq \beta_{rU}$), as the opposite was confirmed to be detrimental to the aeroacoustic performance in prior tests of unducted stacked rotors. These tests were carried out at three different rotational speeds: 3500, 4500 and 5500 RPM. In the second campaign, rotational speed sweeps were carried out for a few key combinations of pitch angles, from 3000 up to 5500 RPM.

Table 1: Relative rotor pitch configurations in the ducted stacked configuration.

$\beta_{rD} - \beta_{rU}$	Relative pitch angles ($\beta_{rU} \backslash \beta_{rD}$)			
0°	$-1°\backslash-1°$	$0°\backslash0°$	$+1°\backslash+1°$	
1°	$-3°\backslash-2°$	$-2°\backslash-1°$	$-1°\backslash0°$	
	$0°\backslash+1°$	$+1°\backslash+2°$	$+2°\backslash+3°$	
2°	$-3°\backslash-1°$	$-2°\backslash0°$	$-1°\backslash+1°$	$0°\backslash+2°$
	$+1°\backslash+3°$			
3°	$-3°\backslash0°$	$-2°\backslash+1°$	$-1°\backslash+2°$	$0°\backslash+3°$
4°	$-3°\backslash+1°$	$-2°\backslash+2°$	$-1°\backslash+3°$	
5°	$-3°\backslash+2°$	$-2°\backslash+3°$		
6°	$-3°\backslash+3°$			

RESULTS AND DISCUSSION

Ducted vs unducted: aerodynamic performance

In this section, the aerodynamic performance of four different rotor configurations is discussed: an isolated rotor, stacked rotors, a single ducted rotor, and stacked ducted rotors. Figure 3 presents the thrust T and thrust coefficient C_T of the four configurations depending on rotational speed. The thrust coefficient is defined as $C_T = \frac{T}{\rho\Omega^2\pi R^4}$, where ρ is air density, Ω is the rotational speed in rad/s, and R is the radius of the propulsion system. For ducted rotors, the total thrust of the rotor+duct system was used, as well as the outer diameter of the duct.

The plots of thrust coefficient in Fig. 3b show an increasing trend, with none of the configurations reaching their maximum thrust coefficient in the measurement range. Adding an additional rotor resulted in a C_T increase of 50-51% without a duct, and 37-41% with a duct. Adding a duct, in turn, yielded a 23-29% increase in thrust coefficient for a single rotor, and 16-18% for stacked rotors. These values depend on a multitude of factors, including blade and duct geometry and axial positioning of the rotors with respect to each other and the duct, so specific conclusions should not be drawn here. Instead, this figure is intended to give an overview of the effectiveness of the different rotor configurations.

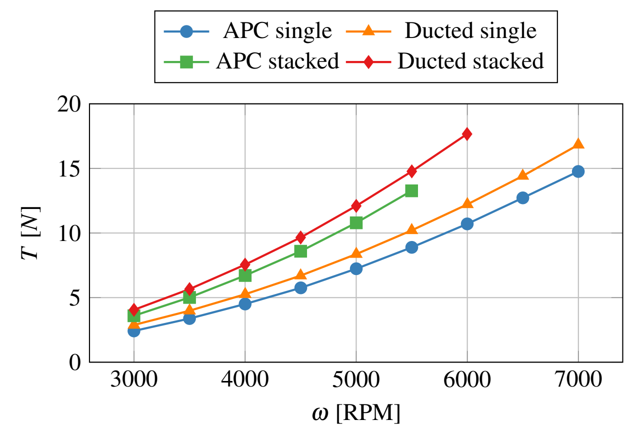

(a) Thrust versus rotational speed.

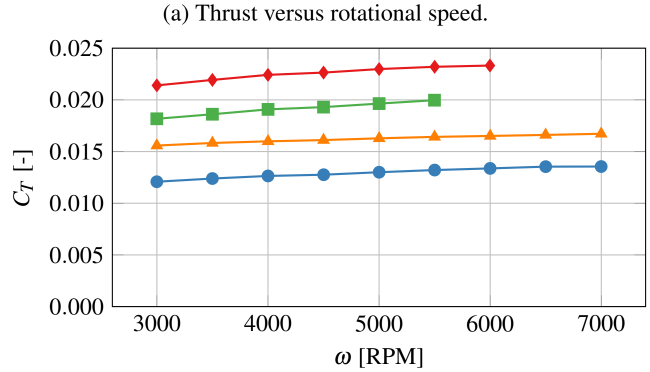

(b) Thrust coefficient versus rotational speed.

Figure 3: Thrust and thrust coefficient of the four rotor configurations.

The plots of thrust versus rotational speed in Fig. 3a reveal no additional information regarding the relative performance of the configurations, as these values also depend on the atmospheric conditions during testing. Furthermore, an additional discrepancy is present due to the different propulsion system radii: $R = 0.15\,\text{m}$ for the ducted rotors, and $R = 0.1524\,\text{m}$ for the APC rotors. However, much of the subsequent analysis of aeroacoustic performance is related to dimensional thrust, as the goal is to provide a lifelike comparison. Therefore, the values of thrust and their variation with rotational speed are provided as a reference.

Aerodynamic efficiency Discussed next are two measures of rotor system efficiency. The figure of merit (FM) is a ratio between the ideal power required to generate a certain amount of thrust and the actual power consumed, and indicates how efficiently the rotor(s) convert their rotational kinetic energy into axial kinetic energy of the air. The figure of merit is defined as $\text{FM} = \frac{C_T^{3/2}}{\sqrt{2}C_Q}$, where $C_Q = \frac{Q}{\rho\Omega^2\pi R^5}$ is the coefficient of torque Q. For ducted rotors, the total thrust of the system and the outer diameter of the duct are taken into account. For ducts with a contraction, which provides additional acceleration to the flow, an alternative form is often used: $\text{FM}\cdot\sqrt{\frac{R_{\text{exit}}}{R_{\text{inner}}}}$, where R_{exit} and R_{inner} are the exit and inner diameters of the duct respectively. However, in the present study the duct has a constant internal diameter ($R_{\text{exit}} = R_{\text{inner}}$), therefore this is equivalent to the traditional definition.

Plots of the figure of merit with respect to thrust are presented in Fig. 4a. The values for the single and stacked APC rotors are similar, indicating the rotors work efficiently in tandem, despite being designed primarily for operation in isolation. In the ducted case, on the other hand, the single rotor has higher values of the figure of merit across the tested range of rotational speeds, and peaks at a higher value of thrust. Regardless of the number of rotors, the addition of a duct results in an improvement in aerodynamic efficiency of the propulsion system between 13% and 23%.

The second efficiency measure discussed here is power loading. This ratio indicates how effectively the propulsion system converts mechanical power into thrust, and is defined as $\text{PL} = \frac{T}{Q\Omega}$. Fig. 4b shows the trends of power loading with respect to thrust for the four rotor configurations. Adding an additional rotor to the system has a negligible impact regardless of the presence of a duct, but adding the duct once again results in an increase in power loading, between 13% and 19% depending on the thrust being generated.

The results for both parameters confirm that the addition of a duct enables more efficient lift generation, by approximately 15% to 20%, for the tested rotor geometries. However, this is at the cost of additional design complexity and weight, with the final trade-off depending on the effectiveness, cost of manufacture, and weight of the duct.

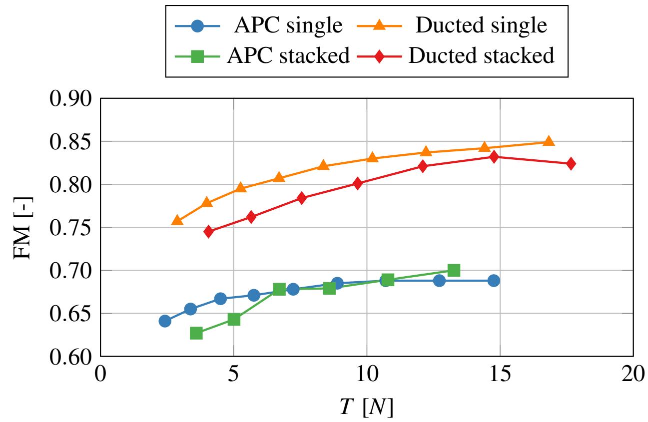

(a) Figure of merit versus thrust.

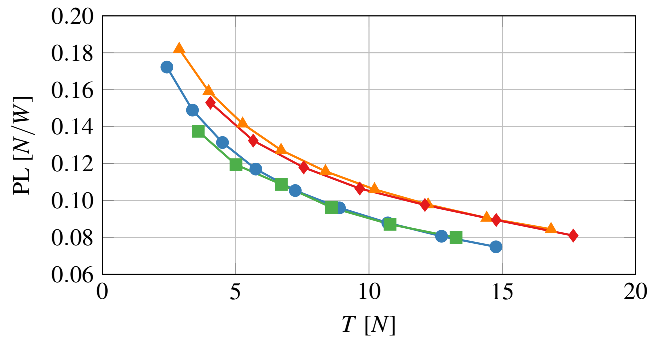

(b) Power loading versus thrust.

Figure 4: Measures of efficiency of the four rotor configurations.

Ducted vs unducted: acoustic performance

Whereas aerodynamic efficiency and weight are the primary concerns in the design process of a propulsion system, acoustic performance is also crucial for many applications. Acoustic emissions and their directivity was measured for all the configurations, at all the data points presented so far. Figure 5 shows the progression with thrust of the overall sound pressure level ($L_{pA,\text{tot}}$), at two different angles: in the rotor plane ($\theta = 0°$), and 40° downstream of the rotor plane ($\theta = -40°$), the latter corresponding to a ground observer. The scale is maintained between the two plots.

The plots of SPL in the rotor plane ($\theta = 0°$) in Fig. 5a show a mixed trend. The single and stacked APC rotors demonstrate similar overall SPL levels up until a thrust of approximately 9 N, above which the single rotor becomes significantly noisier. In the ducted cases, the stacked rotors are consistently noisier than the single rotor at all thrust values, by between 5% and 12%. Across the majority of the thrust range, the single ducted rotor is the quietest configuration, with the ducted stacked and single APC rotor being the noisiest configurations, depending on thrust.

In the downstream position ($\theta = -40°$), which corresponds to a ground observer at a 40° angle to the rotor plane, some changes take place. Notably, the noise levels are increased for all the configurations and at all thrust values. In this position,

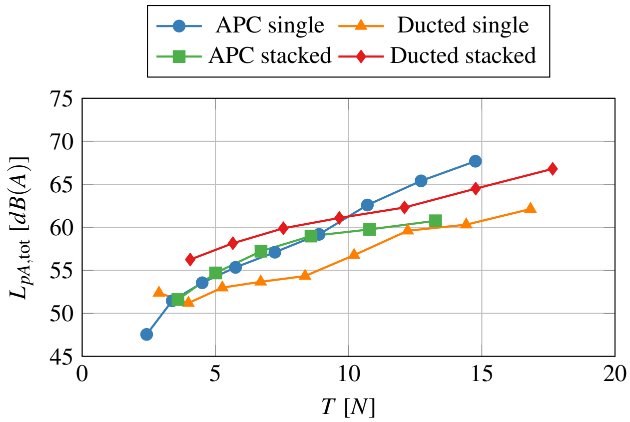

(a) $\theta = 0°$.

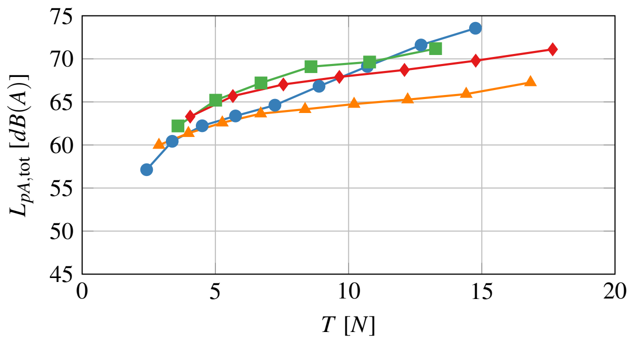

(b) $\theta = -40°$.

Figure 5: Overall sound pressure level with respect to thrust of the four rotor configurations.

the stacked APC rotors are noisier by up to 3 dB than the single APC rotor, and there is less of a difference between the single and stacked ducted rotors. However, the single ducted rotor remains the quietest configuration.

Directivity In order to provide more context about the directivity of the overall sound pressure level emitted by the different rotor configurations, directivity plots at two thrust values are shown in Fig. 6. The first case is for thrust of approximately 7 N, and the second is for thrust between 10.7 N (unducted rotors) and 12 N (ducted rotors). The thrust difference in the second case, which is also the basis for further discussion below, is intended to account for the additional mass of the duct. Naturally, the exact mass of the duct depends on the specifics of every design case, such as permissible manufacturing cost or the required strength, but the intent is to tilt the results in the right direction.

Several distinct trends can be observed in the directivity plots. Firstly, the overall SPL increases with thrust for every configuration and at every observation angle, in line with expectations and the trend apparent in Fig. 5. Secondly, the noise level increases as the observation point moves away from the rotor plane, in most cases at roughly equal rates in the downstream and upstream directions, with the lowest noise levels observed in the rotor plane. The first exception to the downstream-upstream symmetry is the single ducted rotor, which is quieter when observed from the downstream direction. This is caused by the relative location of the rotor and the duct — the rotor is mounted closer to the leading edge of the duct than to its exit, therefore the trailing section of the duct provides more acoustic shielding. However, the second exception is the stacked unducted configuration, and to a lesser extent the single APC rotor, which are quieter when observed from the upstream direction, but only at the angle of $\theta = 20°$. The mechanism responsible for this phenomenon is not known at this stage.

Another notable trend is the inconsistency of the shielding effect of the duct when observed in the plane of the rotor. At $T \approx 7$ N, the single ducted rotor demonstrates a large SPL de-

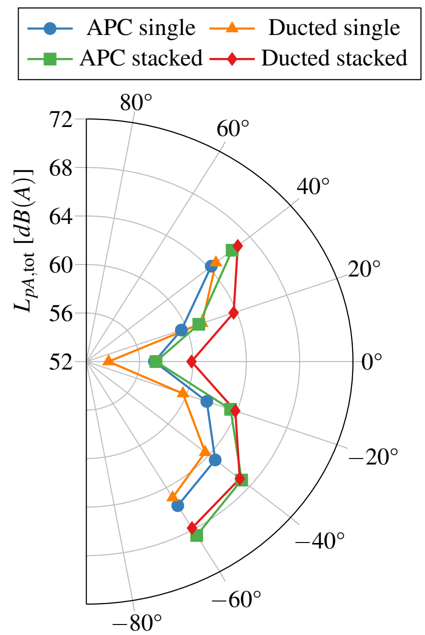

(a) $T \approx 7$ N.

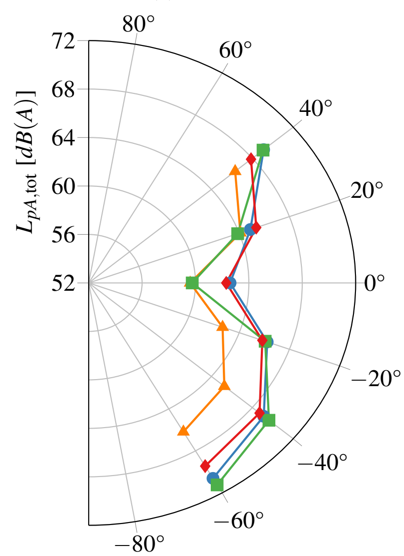

(b) $T \approx 10.7$–12 N.

Figure 6: Directivity plot of the overall sound pressure level of the different rotor configurations, at two thrust levels.

crease at $\theta = 0°$, but the ducted stacked rotors experience a similar change to the unducted rotors. At $T \approx 10.7$–$12\,\mathrm{N}$, the biggest drop in SPL is experienced by the unducted stacked configuration, with the remaining configurations undergoing similar variations. These results indicate that the shielding effect of the duct, while present and noticeable with a single rotor, does not dominate the spatial characteristics of the overall SPL of the ducted propulsion systems. However, it is possible to influence the extent of shielding by extending the ducting in the axial direction, or manufacturing or filling it with a more absorptive material.

Frequency-domain characteristics In order to shed more light on the characteristics of the noise emitted by the different rotor configurations, plots of SPL spectral density of two cases are presented in Fig. 7. The chosen thrust point is the 10.7–12 N for unducted and ducted rotors respectively, whose directivity was illustrated in Fig. 6b. The spectra are shown for two observation angles: $\theta = 0°$ (in-plane) and $\theta = -40°$ (downstream), the same angles as in Fig. 5.

In both cases, the dominant tone is the $2 \cdot \mathrm{RPM}$ harmonic at 200 Hz for the single rotors (corresponding to their blade passing frequency), and at 167 Hz for the stacked rotors. This harmonic is damped significantly in the unducted stacked configuration due to phase cancellation: the oscillating pressure waves from the two rotors are out of phase by a quarter of a revolution, which at the frequency of $2 \cdot \mathrm{RPM}$ corresponds to half of the wavelength. Notably, the phase cancellation effect is not apparent for the ducted stacked configuration; it is possible that the destructive interference becomes distorted as the acoustic waves traverse the body of the duct and diffract around its edges, but it was not possible to verify this as part of these experiments. The next significant tone is the $4 \cdot \mathrm{RPM}$ harmonic, which corresponds to the BPF for the stacked rotor configurations (at 333 Hz), and is the second harmonic of the BPF for the single rotors (at 400 Hz). At $\theta = -40°$, this tone is strongest for the single rotors, in particular for the unducted APC rotor. At $\theta = 0°$, however, it appears to be damped by the duct for the single ducted rotor, but increases in strength for both stacked rotor configurations.

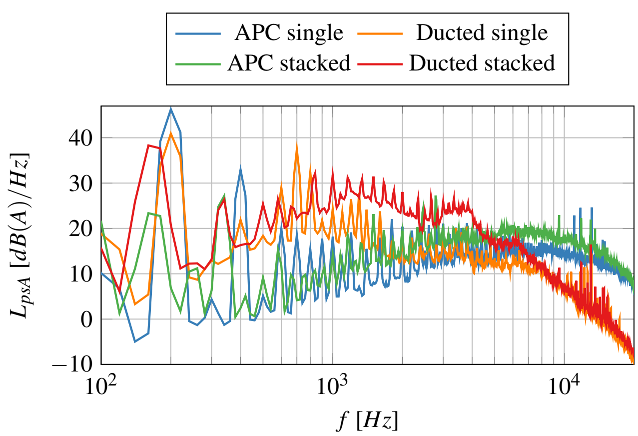

(a) $\theta = 0°$.

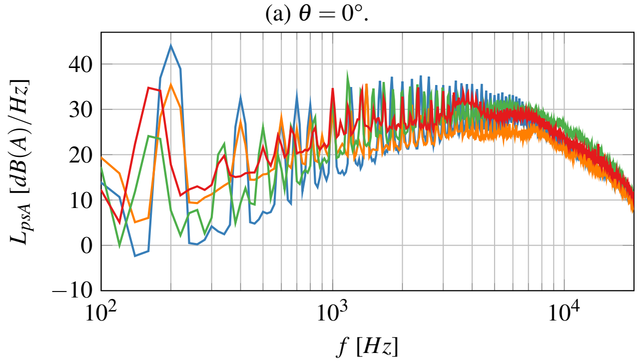

(b) $\theta = -40°$.

Figure 7: Sound pressure spectral density level of the four rotor configuration at thrust values of approximately 10.7 N and 12 N for the unducted and ducted configurations respectively. 20 Hz spectrum resolution.

Spurious noise The dense tonal noise above the $4 \cdot \mathrm{RPM}$ harmonic, i.e. between 500 Hz and 3 kHz, is largely of mechanical nature. One source of the noise is the electric motor itself. However, another are the vibrations of the structure caused by imperfect weight distribution of the motor and rotor assembly, unsteady aerodynamic loads acting on the duct, and acoustic excitation. All these factors introduce vibrations into the structure — both the column supporting the motor and rotor assembly, and the frame supporting the duct. Due to these vibrations, the metal structure of the rig becomes a secondary acoustic source. The duct structure in particular was shown to introduce significant secondary noise, and while attempts were made to alleviate this problem, it was not possible to eliminate it.

Broadband noise Fortunately, the spurious mechanical noise was not sufficiently dense across the frequency spectrum to obscure the broadband noise emitted by the rotors. This can be observed as the "base" of the spectral plots. In the unducted cases, the broadband noise is higher for the stacked rotors by approximately 5 dB across the majority of the spectrum, at both observation angles. However, in both configurations, the broadband noise level is significantly higher when observed from the downstream position ($\theta = -40°$) between 300 Hz and approximately 15 kHz, with a difference of up to 10 dB.

The ducted configurations are characterised by increased broadband noise relative to the respective unducted cases, across most of the frequency spectrum. The ducted configurations also experience a smaller difference between the $\theta = 0°$ and $-40°$ observation angles at moderate frequencies. However, a very clear noise reduction is present at $\theta = 0°$ at high frequencies, beginning at approximately 2 kHz, and reaching a reduction of nearly 20 dB at 20 kHz. This appears to be an effect of acoustic shielding by the duct. However, this high-frequency broadband noise has a relatively small impact on the overall sound pressure level, which is dominated by the RPM harmonics and mid-frequency tonal and broadband noise, which is why it was not apparent in the overall SPL directivity plots in Fig. 6.

Ducted stacked rotors with dissimilar pitch

During the extensive testing of unducted stacked rotor configurations, which is beyond the scope of this work, it was observed that by combining rotors with two different pitch angles — the APC 12x4.5MR (upstream) and the APC 12x5.5MR (downstream) — it was possible to attain a small improvement in aerodynamic efficiency and noise emissions while maintaining the same level of thrust. As the ducted stacked configuration, with its 3D-printed rotor blades, provided more flexibility than the two off-the-shelf variants of the APC rotors, a decision was made to study the effect of dissimilar stacked rotor pitch more extensively. For this purpose, the geometry of the baseline ducted rotor blades was modified, with the core parts of the blades rotated by between $-3°$ and $+3°$ relative to the baseline, which was optimised for single rotor operation. This enabled testing of pitch differences of up to $\Delta\beta_r = 6°$ between the upstream and downstream rotors, and changing the average relative pitch between $\overline{\beta_r} = -2.5°$ and 2.5° (see Table 1).

Aerodynamic performance Figure 8 presents curves of thrust coefficient and figure of merit with respect to the average relative pitch $\overline{\beta_r}$ of the two rotors, obtained at a fixed rotational speed of 4500 RPM. Each colour-coded curve corresponds to a different pitch difference $\Delta\beta_r$ between the two rotors, from 0° (with data points at $-1°\backslash-1°$, $0°\backslash0°$ and $+1°\backslash+1°$), up to 6° ($-3°\backslash+3°$). In other words, the average pitch of the two rotors increases when moving from left to right, and the difference in pitch between the upstream and downstream rotors increases as the colour shifts from blue to red.

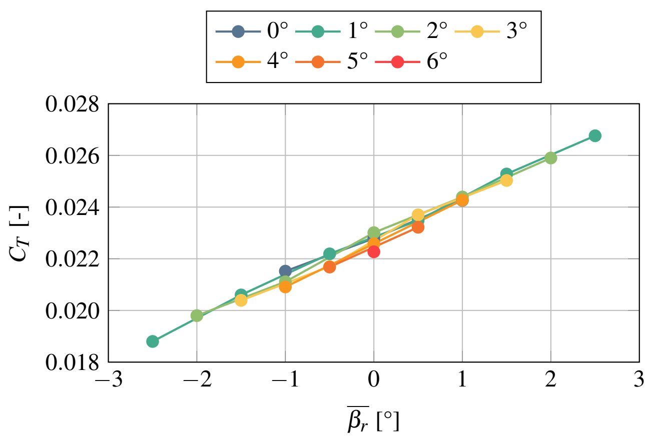

(a) Thrust coefficient versus average relative blade pitch.

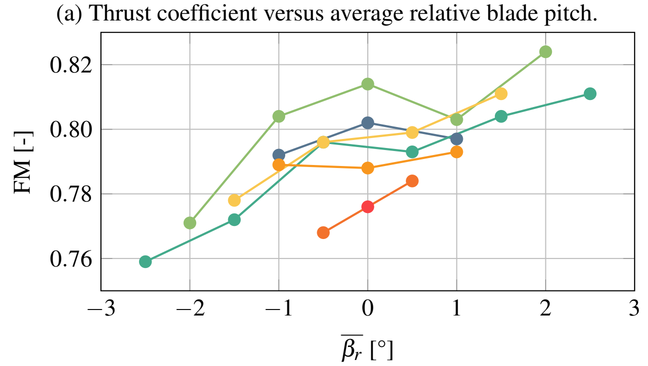

(b) Figure of merit versus average relative blade pitch.

Figure 8: Aerodynamic characteristics of ducted stacked rotors relative to average relative blade pitch at 4500 RPM; each coloured line corresponds to a different pitch difference $\Delta\beta_r$ between the upstream and downstream rotors.

The thrust coefficient curves exhibit a linear increase with increasing average pitch $\overline{\beta_r}$, which, in this narrow range of blade pitch angles, is in line with expectations. The key result is the difference between subsequent curves. Although quantitatively the differences are small, a clear trend can be observed, where increasing the pitch difference $\Delta\beta_r$ between the rotors coincides with a reduction in thrust.

The plots of the figure of merit, illustrated in Fig. 8b, reveal two notable trends. Firstly, the figure of merit broadly increases with increasing average pitch, for all pitch differences. This suggests that while the baseline rotor (with a relative pitch of $\beta_r = 0°$) was optimised for single-rotor operation, the stacked rotor configuration can utilise higher pitch angles more effectively. This is likely due to both rotors experiencing induced axial airflow velocity due to the other rotor, and therefore a reduced effective angle of attack. Secondly, increasing the pitch difference $\Delta\beta_r$ between the rotors has a negligible impact up to 4° (albeit with the 2° pitch difference appearing optimal), with a deterioration in efficiency at higher difference in pitch.

Acoustic performance The next characteristic of ducted stacked rotors with dissimilar pitch is their acoustic performance. The overall sound pressure level is plotted with respect to average relative blade pitch $\overline{\beta_r}$ for the different pitch differences $\Delta\beta_r$ in Fig. 9, in an analogous manner to Fig. 8. As before, two observation angles are considered: in the rotor plane, and 40° downstream ($\theta = -40°$).

The two plots present starkly different trends. At $\theta = 0°$, increasing the average relative blade pitch above $\overline{\beta_r} = -1°$ results in a quasi-linear SPL increase of about 1 dB per degree, regardless of the pitch difference between rotors. Spectral density plots of the SPL, which are omitted here for brevity, reveal this to be caused by a gradual increase in broadband noise (0.1–6 kHz) as the average rotor pitch $\overline{\beta_r}$ is increased. Changing this difference, on the other hand, has a negligible effect on noise levels.

At the downstream position of $\theta = -40°$, however, the 0° average pitch appears to be the optimum in terms of the overall noise level, with the SPL increasing at both lower and higher average pitch angles. Furthermore, there is a clear relationship between the pitch difference $\Delta\beta_r$ and the SPL as well, with higher pitch differences ($-3°\backslash+3°$ in particular) generating a higher SPL. This variation, once again, is caused by a changing level of broadband noise, in this case between 1 kHz and 6 kHz. The difference, however, is relatively small, with the highest ($-3°\backslash+3°$) and lowest ($0°\backslash0°$) pitch differences separated by less than 1 dB.

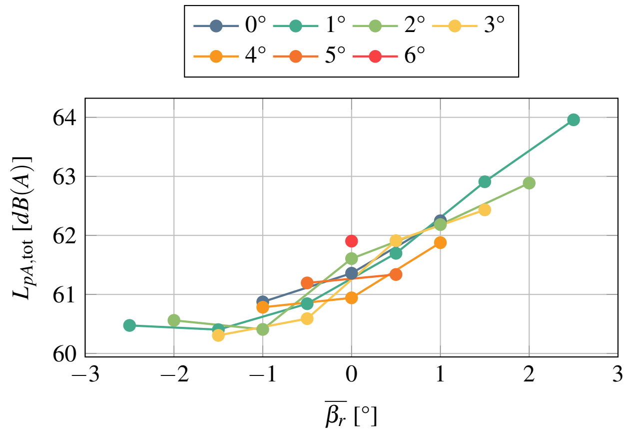

(a) $\theta = 0°$.

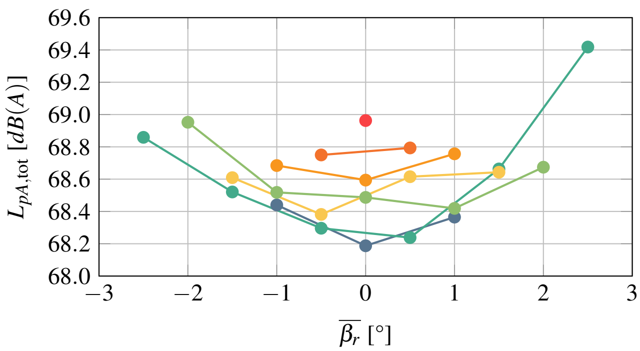

(b) $\theta = -40°$.

Figure 9: Overall sound pressure level of ducted stacked rotors relative to average relative blade pitch at 4500 RPM; each coloured line corresponds to a different pitch difference $\Delta\beta_r$ between the upstream and downstream rotors.

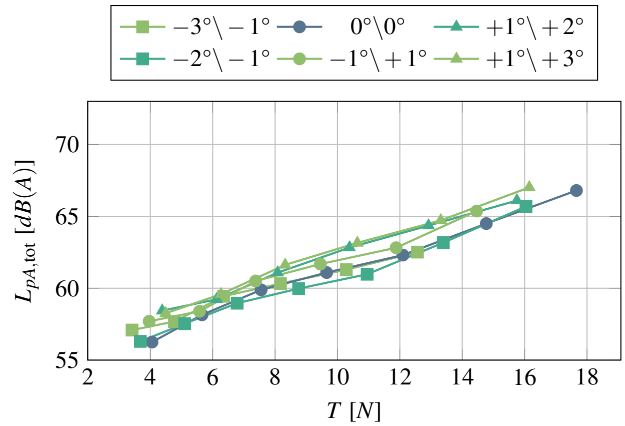

(a) $\theta = 0°$.

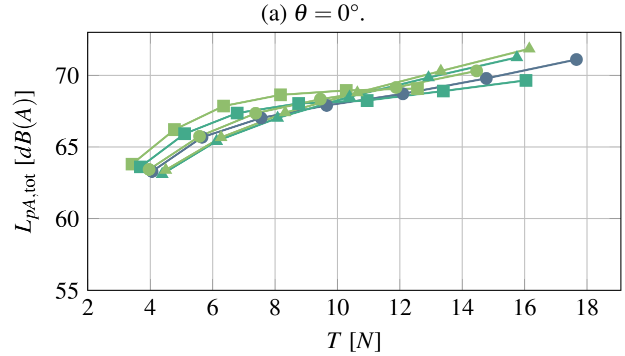

(b) $\theta = -40°$.

Figure 10: Overall sound pressure level versus thrust for selected rotor pitch configurations of a ducted stacked rotor system; colours correspond to Figures 8 and 9.

Dissimilar rotor pitch vs thrust Finally, plots of the overall sound pressure level with respect to thrust are shown in Fig. 10 for selected rotor pitch configurations, in order to enable assessment of their acoustic performance at corresponding operating conditions. As previously, the overall SPL at two locations is plotted: $\theta = 0°$ and $\theta = -40°$.

In line with the results plotted in Fig. 5, monotonic increase of SPL with thrust occurs for all rotor pitch configurations, with higher values and a more pronounced change in gradient at $\theta = -40°$. The differences between particular configurations reach up to 3 dB at both observation angles, but the trends with respect to $\overline{\beta_r}$ and $\Delta\beta_r$ depend on both the observation angle and on thrust.

In the rotor plane, i.e. at $\theta = 0°$, the high-pitch configurations ($\overline{\beta_r} > 0$, denoted by triangles) are consistently the loudest, whereas the low-pitch configurations ($\overline{\beta_r} < 0$, denoted by squares) and the baseline configuration ($0°\backslash0°$) are the quietest, with $-1°\backslash+1°$ located in the middle. The differences between the loudest and quietest configurations are relatively constant with respect to thrust, and vary between 1 dB and 3 dB.

Downstream of the rotor plane, i.e. at $\theta = -40°$, the trend reverses at $T \approx 11$ N. Above this value, the high-pitch configurations are the loudest once again, with $-2°\backslash-1°$ and $0°\backslash0°$ producing the lowest SPL. However, below this thrust threshold, the low-pitch configurations become the loudest, with the $\overline{\beta_r} > 0$ configurations yielding the lowest noise levels.

These results confirm that the relative pitch angles of both rotors have a significant impact on the noise emissions of the ducted stacked rotor propulsion system, providing an incentive for their optimisation. Furthermore, they show that the optimal rotor configuration depends on the expected operating conditions, such as altitude (which impacts typical observer angles) and thrust or disk loading.

CONCLUSIONS

This study presented a systematic experimental investigation into the aeroacoustic performance of several configurations of rotor-based UAV propulsion in hover. Four distinctive configurations were evaluated: an isolated rotor, stacked rotors, a single ducted rotor, and stacked ducted rotors. Additionally, the influence of dissimilar blade pitch between the upstream and downstream rotors in the ducted stacked configuration was investigated. The results provide insight into the aerodynamic and acoustic performance of each configuration, with implications for UAV design in noise-sensitive applications.

The core findings of this work can be summarised as follows:

1. The addition of a second rotor increases thrust, and therefore disk loading, by approximately 50% in the unducted case and 40% with a duct, at a given rotational speed. In addition, single and stacked ducted rotors produce approximately 25% and 17% more thrust than their unducted counterparts. This suggests that the stacked ducted configuration is particularly advantageous for compact multirotor designs.

2. Ducted rotors also offer improved aerodynamic efficiency compared to the single and stacked unducted rotors, with an increase in the figure of merit and power loading of approximately 15–20%. However, this gain is offset by the increased mechanical complexity and weight of the duct and its supporting structure.

3. Acoustically, the single ducted rotor is the quietest configuration across most operating conditions, especially in the rotor plane and at downstream observer angles. The stacked ducted rotors exhibit overall sound pressure level higher by 5–12%, depending on thrust and observation angle. The unducted configurations produce noise levels similar to each other and in a similar range to the ducted stacked rotors, once again depending on thrust and observation angle.

4. The duct provides partial acoustic shielding, and is particularly effective at frequencies above 5 kHz. However, it appears to disrupt the phase cancellation effect of the stacked rotors, with the $2 \cdot \text{RPM}$ tone not damped significantly, unlike in the unducted stacked configuration. It also appears that the axial position of the rotor(s) within the duct is of high importance, with upstream positioning of the single ducted rotor resulting in the most effective acoustic shielding in the downstream direction.

5. In all the configurations, the overall sound pressure level is dominated by mid-frequency tonal and broadband noise, but harmonics of the rotational speed of the rotors, including the blade-passing frequency, are significant due to their annoyance factor. The unducted stacked configuration exhibits the weakest tone at the frequency of $2 \cdot \text{RPM}$, which is the most distinct tone across the spectrum.

6. Introducing dissimilar blade pitch between the upstream and downstream rotors in the ducted stacked configuration has a measurable but modest impact. Aerodynamically, small pitch differences (up to $2°$) can yield a slight improvement in efficiency, while larger differences degrade performance. Acoustically, certain pitch combinations reduce the overall sound pressure level by up to 1–3 dB, depending on thrust and observer angle.

7. The optimal rotor configuration depends on the intended operating conditions, including the required thrust, expected altitude and observer positions, and noise constraints. This highlights the importance of tailored design and optimisation for specific UAV applications, including the individual rotors in the stacked configuration.

To conclude, the findings presented herein demonstrate the potential of ducted stacked rotors as a viable propulsion solution for UAVs, particularly where compactness and efficiency are priorities. However, further research is needed to refine duct and rotor geometries, explore dynamic flight conditions, and develop noise mitigation strategies tailored to coaxial ducted systems.

Author contact:
Pawel.Kekus-Kumor@ilot.lukasiewicz.gov.pl
Adam.Sieradzki@ilot.lukasiewicz.gov.pl

ACKNOWLEDGMENTS

The work described in this paper was carried out as part of the INTERNOISE project at the Łukasiewicz Research Network — Institute of Aviation.

The authors would like to acknowledge Witold Klimczyk for his numerical and optimisation work, which was an integral part of the project and contributed to the results described in this paper.

REFERENCES

1. A. Christian and R. Cabell, “Initial investigation into the psychoacoustic properties of small unmanned aerial system noise,” in *23rd AIAA/CEAS Aeroacoustics Conference*, no. AIAA 2017-4051. Denver, CO, USA: American Institute of Aeronautics and Astronautics, 5-9 June 2017.

2. O. Barbara, L. Seth, A. Roalt, D. Schreckenberg, and M. van Miltenburg, “Association between short-term annoyance and several physiological parameters during different amounts of nocturnal aircraft noise exposure,” *Transactions on Aerospace Research*, vol. 2020, no. 4, 2020.

3. L. Leylekian, M. Lebrun, and P. Lempereur, “An overview of aircraft noise reduction technologies,” *Aerospace Lab*, vol. 6, 2014.

4. P. Candeloro, D. Ragni, and T. Pagliaroli, “Small-scale rotor aeroacoustics for drone propulsion: a review of noise sources and control strategies,” *Fluids*, vol. 7, no. 8, p. 279, 2022.

5. D. Casalino, E. Grande, G. Romani, D. Ragni, and F. Avallone, “Definition of a benchmark for low reynolds number propeller aeroacoustics,” *Aerospace Science and Technology*, vol. 113, p. 106707, 2021.

6. E. Grande, G. Romani, D. Ragni, F. Avallone, and D. Casalino, “Aeroacoustic investigation of a propeller operating at low Reynolds numbers,” *AIAA Journal*, vol. 60, no. 2, pp. 860–871, 2022.

7. S. Whiteside, N. Zawodny, X. Fei, N. A. Pettingill, M. D. Patterson, and P. Rothhaar, "An exploration of the performance and acoustic characteristics of UAV-scale stacked rotor configurations," in *AIAA Science and Technology Forum 2019*, San Diego, CA, USA, 7-11 January 2019, paper No. AIAA 2019-1071.

8. C. Tinney and J. Valdez, "Thrust and acoustic performance of small-scale, coaxial, corotating rotors in hover," *AIAA Journal*, vol. 58, no. 4, pp. 1657–1667, 2020.

9. Y.-B. Lee and J.-S. Park, "Hover performance analyses of coaxial co-rotating rotors for eVTOL aircraft," *Aerospace*, vol. 9, no. 3, p. 152, 2022.

10. W. Klimczyk, P. Kekus-Kumor, and A. Sieradzki, "Experimental validation of vortex particle method for modeling of rotor interaction noise," in *Proceedings of the 30th AIAA/CEAS Aeroacoustics Conference (2024)*, Rome, Italy, 4-7 June 2024.

11. R. McKay, M. Kingan, S. T. Go, and R. Jung, "Experimental and analytical investigation of contra-rotating multi-rotor UAV propeller noise," *Applied Acoustics*, vol. 177, p. 107850, 2021.

12. S. Zhong, Z. Ma, P. Zhou, H. Wu, and X. Zhang, "Predicting the aerodynamic noise of counter-rotating coaxial rotors," *Journal of Sound and Vibration*, vol. 547, p. 117487, 2023.

13. S. Yilmaz, D. Erdem, and M. Kavsaoglu, "Performance of a ducted propeller designed for UAV applications at zero angle of attack flight: An experimental study," *Aerospace Science and Technology*, vol. 45, pp. 376–386, 2015.

14. H. Wang, Y. Wang, S. Wang, and F. Zhou, "Optimization strategy for performance improvement of a lift fan cowl lip based on panel method," *Journal of Mechanical Science and Technology*, vol. 35, no. 7, pp. 2961–2970, 2021.

15. A. M. Malgoezar, A. Vieira, M. Snellen, D. G. Simons, and L. L. Veldhuis, "Experimental characterization of noise radiation from a ducted propeller of an unmanned aerial vehicle," *International Journal of Aeroacoustics*, vol. 18, no. 4-5, pp. 372–391, 2019.

16. J. Guo, T. Zhou, Y. Fang, and X. Zhang, "Experimental study on a compact lined circular duct for small-scale propeller noise reduction," *Applied Acoustics*, vol. 179, p. 108062, 2021.

17. F. Simon, N. H. Schiller, N. S. Zawodny, N. A. Pettingill, and M. B. Galles, "Fundamental noise characterization of a ducted propeller in hover," in *51st International Congress and Exposition on Noise Control Engineering (Inter-noise 2022)*, Glasgow, UK, 21-24 August 2022.

18. T. Zhang and G. N. Barakos, "Review on ducted fans for compound rotorcraft," *The Aeronautical Journal*, vol. 124, no. 1277, pp. 941–974, 2020.

19. F. Avallone, D. Ragni, and D. Casalino, "On the effect of the tip-clearance ratio on the aeroacoustics of a diffuser-augmented wind turbine," *Renewable Energy*, vol. 152, pp. 1317–1327, 2020.

20. Z. Wang, Q. Henricks, M. Zhuang, A. Pandey, M. Sutkowy, B. Harter, M. McCrink, and J. Gregory, "Impact of rotor–airframe orientation on the aerodynamic and aeroacoustic characteristics of small unmanned aerial systems," *Drones*, vol. 3, p. 56, 2019.

21. P. Kekus-Kumor and A. Sieradzki, "Experimental investigation of unmanned air vehicle rotor aeroacoustics using benchmark geometries," in *Proceedings of the 52nd International Congress and Exposition on Noise Control Engineering (Inter-noise 2023)*, Chiba, Japan, 20-23 August 2023.

22. P. Kekus-Kumor and A. Sieradzki, "A low-cost anechoic chamber for rotor aeroacoustics research: Design and validation," *Transactions on Aerospace Research*, vol. 2025, no. 2, pp. 18–39, 2025.

23. A. Sieradzki, P. Kekus-Kumor, and W. Klimczyk, "Potential of unconventional low-noise propulsion designs for UAV/UAM applications," in *Proceedings of the 50th European Rotorcraft Forum (2024)*, Marseille, France, 10-12 September 2024.